AIP Advances

Tuning of undoped ZnO thin film via plasma enhanced atomic layer deposition and its application for an inverted polymer solar cell

Mi-jin Jin, Junhyeon Jo, Guru P. Neupane, Jeongyong Kim, Ki-Seok An, and Jung-Woo Yoo

Citation: AIP Advances **3**, 102114 (2013); doi: 10.1063/1.4825230
View online: http://dx.doi.org/10.1063/1.4825230
View Table of Contents: http://scitation.aip.org/content/aip/journal/adva/3/10?ver=pdfcov
Published by the AIP Publishing

Tuning of undoped ZnO thin film via plasma enhanced atomic layer deposition and its application for an inverted polymer solar cell

Mi-jin Jin,[1] Junhyeon Jo,[1] Guru P. Neupane,[2] Jeongyong Kim,[2] Ki-Seok An,[3] and Jung-Woo Yoo[1]

[1]*School of Mechanical and Advanced Material Engineering-Low dimensional Carbon Materials Center, Ulsan National Institute of Science and Technology, Ulsan, 688-798, Republic of Korea*

[2]*Department of Energy Science and IBS Center for Integrated Nanostructure Physics, Sungkyunkwan University, Suwon 440-746, Republic of Korea*

[3]*Thin Film Materials Research Group, Korea Research Institute of Chemical Technology, Daejeon, 305-543, Republic of Korea*

(Received 24 July 2013; accepted 26 September 2013; published online 10 October 2013)

We studied the tuning of structural and optical properties of ZnO thin film and its correlation to the efficiency of inverted solar cell using plasma-enhanced atomic layer deposition (PEALD). The sequential injection of DEZn and O_2 plasma was employed for the plasma-enhanced atomic layer deposition of ZnO thin film. As the growth temperature of ZnO film was increased from 100 °C to 300 °C, the crystallinity of ZnO film was improved from amorphous to highly ordered (002) direction ploy-crystal due to self crystallization. Increasing oxygen plasma time in PEALD process also introduces growing of hexagonal wurtzite phase of ZnO nanocrystal. Excess of oxygen plasma time induces enhanced deep level emission band (500 $\sim$ 700 nm) in photoluminescence due to Zn vacancies and other defects. The evolution of structural and optical properties of PEALD ZnO films also involves in change of electrical conductivity by 3 orders of magnitude. The highly tunable PEALD ZnO thin films were employed as the electron conductive layers in inverted polymer solar cells. Our study indicates that both structural and optical properties rather than electrical conductivities of ZnO films play more important role for the effective charge collection in photovoltaic device operation. The ability to tune the materials properties of *undoped* ZnO films via PEALD should extend their functionality over the wide range of advanced electronic applications. [http://dx.doi.org/10.1063/1.4825230]

I. INTRODUCTION

ZnO, one of the most attractive metal oxides, has been under intense research due to a variety of potential value in use. It (wurtzite structure) has band gap energy of 3.37 eV and excitonic binding energy of 60 meV and exhibits semiconducting,[1] opto-electric,[2–6] piezo-electric,[7–12] and pyro-electric properties.[13–16] Especially, controllable *n*-type, *p*-type semiconductor properties of ZnO film are well suited for many of device applications, such as electronics, optoelectronics, sensors, and the biological sciences.[17–23] A variety of methods have been established for the growth of ZnO thin films. Atomic layer deposition is one of the most attractive methods for the growth of ZnO thin film due to its simplicity, reproducibility, and highly conformal growth.[24–30] This layer-by-layer growth method can also make it easier to obtain highly ordered poly-crystal and/or very homogeneous film. And the surface controlled deposition characteristic allows high-aspect ratio deposition, which is suitable for various nano-structured electronic applications.

It is highly important to obtain facile tuning of ZnO thin film to meet the necessaries of various device applications with desired materials properties. Doping of ZnO is straightforward approach to tune its materials properties.[31–37] However, doping is generally difficult to control and reproduce. In fact, the materials properties of ZnO highly depend on the growth conditions, such as oxygen levels, impurities, growth rate and temperature, and even post annealing. Oxygen vacancies or impurities can create deep level states between valence band and conduction band, which directly or indirectly affect electronic properties of films, such as mobility, conductivity, optical absorption etc.[25,37–39] Several studies of thermal-ALD and PEALD showed that the conductivity of ZnO film can be easily tuned by controlling the growth temperature and plasma time.[25,40–42] For the optoelectronic applications of ZnO film, not only the electrical properties but also the structural and optical properties of ZnO film can also be very important factors for optimal device performance. It is important to establish the control of structural and optical properties of ZnO film and how the changes in such properties affect on the device applications.

One of the optoelectronic applications of ZnO films is using them as the electron conductive layers in inverted polymer solar cells.[43] Unlike conventional polymer solar cell, the generated electrons are collected at ITO cathode, whereas the generated holes are collected at top metal electrode in inverted polymer solar cell.[44–46] One of the key elements to enhance efficiency of inverted polymer solar cells is the effective collection of generated charge by the insertion of electron conductive layer (or hole barrier) and hole conductive layer (or electron barrier) between active layer and electrodes (cathode and anode).[44–46] These buffer layers help to maintain open circuit voltage, improve charge selectivity, and alleviate electron-hole recombination. ZnO films grown by sol-gel methods have been widely used as an electron conductive layer in this device configuration.[31,33,34,36,43,47] Enhanced electrical conductivity of ZnO film may improve the performance of electron conductive ZnO layer in inverted polymer solar cell. By introducing a variety of methods of doping, several studies have focused on improving electrical conductivities of ZnO films for the applications of inverted polymer solar cells.[31,33,34,36] Generally, ZnO grown by thermal ALD method provide better quality of film than ZnO grown by sol-gel method with improved structural order. While both the sol-gel and ALD growth of ZnO require high temperature processing, the PEALD method allows us to grow high-quality ZnO film at relatively low temperature. Therefore, it is well suitable for the flexible solar cell technology, which is one of the main advantages of polymer solar cell over inorganic solar cells. The ability to control of surface morphology and crystal structure of electron conductive thin film (hole barrier) between active layer and electrode would be important factor to improve photovoltaic performance because increased surface area (morphology control) can increase short circuit current and improved crystallinity aids to avoid unwanted charge trapping.[3,31,48,49] The electronic structure of ZnO thin film is also an essential property to function as an electron conductive layer (or hole barrier). It helps to maintain charge selectivity and open circuit voltage in inverted polymer cell. Therefore, it is highly desirable to achieve simple tuning of structural and optical properties of ZnO thin film for polymer solar cells and other optoelectronic applications.

In this work, we studied how the materials properties of ZnO thin film are associated with the PEALD growth conditions and their impact on the device performance. The surface morphology, crystallinity, optical band, and conductivity of *undoped* ZnO film were all highly dependent on the substrate temperature and O_2 plasma time in PEALD process. The device performances of these highly tunable ZnO thin films were tested by incorporating them into the polymer solar cells. Improving conductivity of ZnO film can be presumed to improve electron collection of ZnO layer in inverted polymer solar cell. However, our results showed that maintaining electronic structure of ZnO film is more important factor to improve photovoltaic device performance. The inverted polymer solar cell with an optimized PEALD ZnO thin film growth condition showed maximum efficiency of 4.08 % (J_{sc} = 13.28 mA/cm^2, V_{oc} = 0.49 V, Fill Factor = 0.53) under A.M (air mass) 1.5 G illumination.

II. EXPERIMENTAL

All ZnO thin films were grown on ITO/Glass substrates, which were used further as the cathodes of polymer solar cells. Substrate was cleaned with de-ionized water, acetone, ethanol in ~41 kHz

TABLE I. PEALD growth conditions for 1cycle of PEALD process. (Ar gas flow rate for DEZn precursor or purging: 10 sccm, RF plasma power: 180 W, Ar gas flow rate for plasma: 5–7 sccm, Oxygen gas flow rate for plasma: 1 sccm).

Sample Condition	No.	Substrate temp.	DEZn pulse [s]	DEZn purge [s]	O_2 plasma [s]	O_2 plasma purge [s]
Substrate temp.	1	100 °C				
	2	150 °C				
	3	200 °C			20	
	4	250 °C				
	5	300 °C				
			0.01	50		30
Oxygen plasma time	1				10	
	2				20	
	3	200 °C			30	
	4				40	
	5				50	

ultrasonic cleaner bath for 30min in sequence. SVT associates Inc's Plasma Enhanced Atomic Layer Deposition (PEALD) system was used for ZnO thin film growth. Diethyl-zinc (DEZn) was used as a Zn precursor followed by Argon assisted oxygen plasma step for oxidation (oxygen source). Sample stage temperature of the PEALD chamber was maintained at 100 °C, 200 °C, and 300 °C to see the different film growth behavior. But source purging line was maintained at 100 °C for all batches of samples. DEZn source was maintained at room temperature. The source carrier gas (Ar) flow rate was 5-7 sccm (Standard Cubic Centimeter per Minute). The Ar gas and oxygen gas flow rates for argon assisted oxygen plasma were 10 sccm and 1sccm, respectively. 180 W of RF (radio frequency, 13.56 MHz) power was applied for oxygen plasma. For 1 cycle of ZnO layer growth, DEZn precursor was first injected for 0.01s and then purged with Ar gas for 50 sec to remove residues and other impurities. Then, Ar assisted oxygen plasma was ignited and maintained for 10-50 sec. Finally, the chamber was purged with Ar carrier gas (5-7 sccm) to remove remained oxygen gases. The growth conditions of PEALD ZnO films are summarized in Table I.

The thicknesses of ZnO films were measured by alpha step instrument. Although the profilometer can only provide rough estimation of the film thickness, typical thicknesses of ZnO films grown by 100 cycles of PEALD were ~25 nm (~0.25 nm/cycle of growth rate). The variation of film thickness depending on plasma time and substrate temperature was nominal without general trend. The sheet resistances of samples were tested by using four probe measurement. The surface image and morphology of ZnO thin film were taken by Field Emission Scanning Electron Microscopy (FE-SEM) and tapping mode of Atomic Force Microscopy (AFM), respectively. Crystal growth direction and structure of a ZnO thin film were analyzed using X-ray diffraction (XRD). (002) diffraction peak of ZnO thin film starts to develop when the growth temperature was maintained over 200 °C (Fig. 2(a)). Increasing oxygen plasma time in PEALD process over 20 sec also enhanced (002) peak of ZnO thin film (Fig. 2(b)). Photoluminescence (PL) spectra were measured at room temperature utilizing the 355 nm line with 0.3 sec exposure time and 0.1 sec acquistion time. To see an effect of ZnO thin film's crystal quality and optical property on the application of electronic devices, we fabricated inverted type polymer solar cell using ZnO layer as an electron conductive buffer layer. All ZnO thin films were grown on ITO/Glass substrates, which were used as the transparent conductive bottom electrodes. P3HT (poly(3-hexylthiophene), Regio-regularity 98%) : PCBM (Phenyl-C71-butyric acid methyl ester) bulk heterojunction layer was used as an active layer. P3HT:PCBM with 1:1 mass ratio was dissolved in 2 ml Clorobenzene (99.8%) solution and then spin coated on ZnO thin film/ITO/Glass substrate with thickness of ~200 nm. Then, MoO_x(5 nm)/Au(60 nm) layers were thermally deposited in step for the hole conducting layer. The photovoltaic effects were tested by using solar simulator (Abet technology, Xenon lamp) and *I-V* measurement system (IVIUM technologies) upon A.M 1.5 mass illumination (100 mW/cm^2).

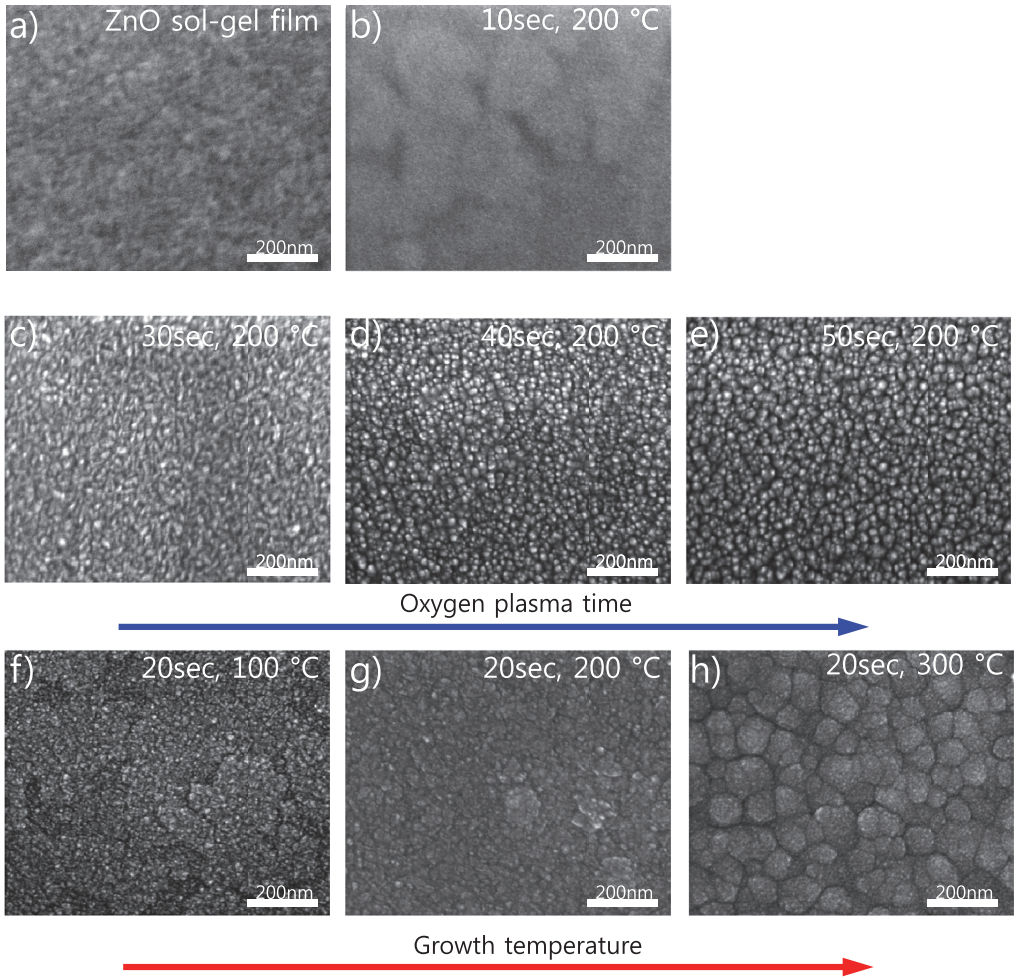

FIG. 1. (a) FE-SEM image of ZnO sol-gel film. (b)–(e) FE-SEM images depending on oxygen plasma ignition time at 200 °C substrate temperature. When plasma time is too small (10 sec), there are few interaction between Zn & O (crystals or nuclei are not shown). As the plasma time is increased, ZnO nanocrystals start to nucleate. (f)-(g) FE-SEM images depending on substrate temperature variation at 20 sec O_2 plasma time. As the growth temperature is increased, ZnO nano crystals aggregrate to form larger grains with distinct grain boundaries.

III. RESULTS AND DISCUSSION

All ZnO thin films studied as well as ZnO films used for polymer solar cells in this paper were grown by 100 cycles of PEALD process. Fig. 1 shows FE-SEM images displaying the surface morphology of the ZnO films deposited on the ITO/Glass substrate with different growth temperature (Fig. 1(c)–1(e)) and different plasma time (Fig. 1(f)–1(h)) of PEALD method, respectively. FE-SEM image of ZnO sol-gel film was also shown in Fig. 1(a) to compare surface morphology. They are all highly uniform and maintain low surface roughness variation (1–2 nm). As can be seen in Fig. 1(b), ZnO thin film grown with 10 sec of oxygen plasma time and 200 °C substrate temperature displays no crystal structure or grain boundary, similar to the ZnO sol-gel film (Fig. 1(a)). But, with sufficient oxygen plasma time, vertically oriented nano-size crystals started to develop on the surface of ZnO thin films. As the plasma time was increased from 30 sec to 50 sec (see Fig. 1(c)–1(e)), the nano crystals on ZnO thin films grew in size and surface morphologies of films displayed corn-like shape structure. A variety of the crystalline growth of ALD films from different initial seeds were previously studied.[24] The size of ZnO nano crystal grown with 20 sec plasma time for all different growth temperature (Fig. 1(f)–1(h)) is typically smaller than that of ZnO nano crystal grown with longer plasma time 30 sec ∼ 50 sec (Fig. 1(c)–1(e)). This suggests O_2 plasma assists nucleation

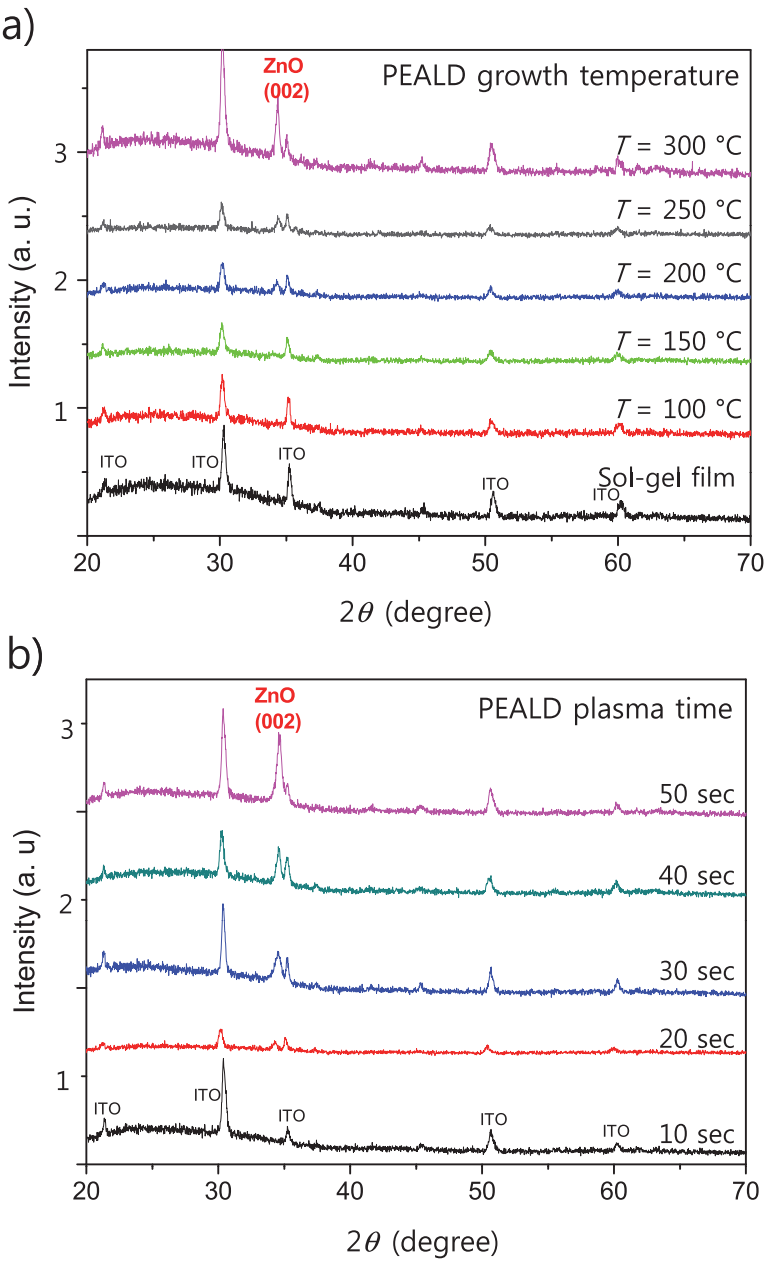

FIG. 2. (a) XRD patterns of PEALD ZnO films depending on growth temperature from 100 to 300 °C with 50 °C interval. XRD pattern of ZnO sol-gel film is also included for comparison. As the growth temperature is increased, (002) peak for the hexagonal wurzite phase of ZnO gradually develops. (b) XRD patterns of PEALD ZnO films for the variation of O_2 plasma time from 10 sec to 50 sec with 10 sec interval. Increasing plasma time also enhances (002) directional crystallinity.

of various size of single crystals that are more vertically oriented.[24] And in proportion to substrate temperature from 100 °C to 300 °C, ZnO nano-crystals were merged together with neighbor ZnO nano-crystals by the thermal energy and gradually grew in size with distinct grain boundaries (see Fig. 1(f)–1(h)) Therefore, during the ZnO film growth at high enough substrate temperature, both chemical reaction of DEZn with oxygen and thermal reaction among ZnO seed crystal are present in PEALD process.

Fig. 2 shows the X-ray diffraction patterns of the ZnO films deposited on the ITO/Glass substrates at different temperatures (a) and at different O_2 plasma times (b) with 100 PEALD cycles. The ZnO

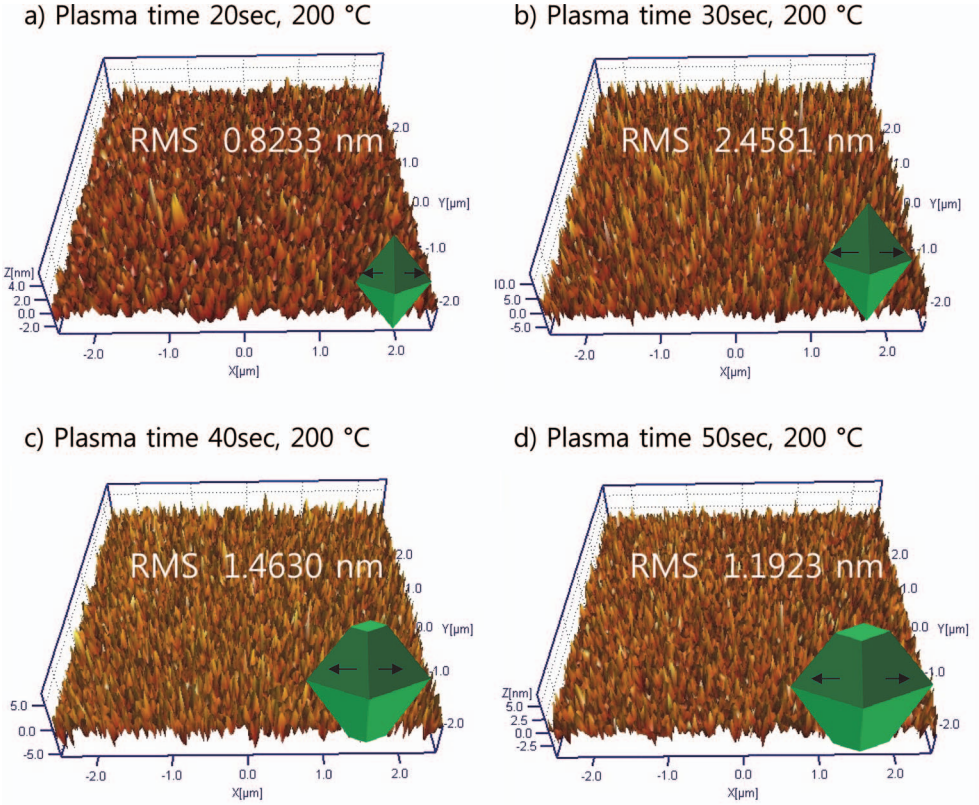

FIG. 3. Atomic Force Microscopy images of ZnO thin films for the variation of O_2 plasma time. RMS (root mean squire) roughness values are also indicated in the figure. The evolution of nanocrystal growth is also illustrated in figure with green polyhedrons. The surface morphology and RMS roughness well follow growth dynamics simulated by Ola Nilsen *et al*.[50]

films grown on ITO substrates showed only a (002) preferred orientation over the entire range of our deposition conditions except for amorphous samples (100 °C growth temperature sample and 10 sec of oxygen plasma time sample). As can be seen in Fig. 2(a), XRD peaks of ZnO thin films were not found for the samples grown at 100 °C and 150 °C as well as the samples grown by sol-gel method. With increasing growth temperature over 200 °C, samples displayed (002) peaks for the hexagonal wurzite phase of ZnO thin films. The PEALD ZnO thin films were also developed into the same crystal phase with (002) peak by increasing oxygen plasma time. Fig. 2(b) displays that (002) diffraction peak became more apparent as we increased oxygen plasma time up to 50 sec in PEALD process. Overall, both increasing growth temperature and plasma ignition time result in a better crystallographic structure of ZnO thin film with enhanced single (002) orientation and larger grains.

Fig. 3 shows Atomic Force Microscopy (AFM) topographic images of PEALD ZnO thin films grown with different O_2 plasma times (20, 30, 40, and 50 sec). All samples display relatively homogeneous thin films with small variation of Root Mean Square (RMS) roughness 0.82 $\sim$ 2.45 nm. Both FE-SEM images (Fig. 1) and AFM images (Fig. 3) of ZnO films suggest that the nano-sized ZnO crystals start to develop and increase in size with increasing plasma time up to 30 sec. Then, ZnO crystal grains continue to expand more with increasing plasma time further. The growth dynamics of polycrystalline films in atomic layer deposition were thoroughly studied by Ola Nilsen *et al*.[50] According to their simulation, initial structure of nano-crystal will determine surface morphology and crystal growth direction with open plane site. The crystal growth of our ZnO thin films are illustrated as polyhedrons in inset of Fig. 3, which are well correspond to the simulation of Ola Nilsen. The evolution of ZnO surface roughness also well follows this model of growth dynamics. As indicated in Fig. 3, ZnO surface roughness initially increased and then started

to decrease at some point with the growth of crystal grains. Generally, increase of film surface roughness leads to increase of effective surface area. In our ZnO thin films, the sample grown with plasma time of 30 sec is expected to have largest effective surface area.

A numder of studies indicate that the conductivity of ZnO thin film largely depends on native defect concentrations.[51,52] In addition, interstitial impurities (such as C, H come from precursor DEZn), induced from ALD process can significantly affect electrical conductivity and optical property of ZnO film. Photoluminescence (PL) spectra for a series of ZnO thin film samples were measured to see both the direct band gap and deep levels from defects in ZnO thin films. Fig. 4(a) and 4(b) shows PL spectra of PEALD ZnO thin films with different growth conditions. All PL spectra display the well-known excitonic emission band peak of ZnO near the ∼384 nm wavelength (∼3.24 eV), which can be attributed to the recombination of free excitons.[38,53,54] And the deep level emission of broad region (500 ∼ 700 nm) is known to be related to the presence of the slightly ionized oxygen vacancies or other point defects.[38,54,55] The intensities of broad emission band from deep level slightly increase with increasing growth temperature (Fig. 4(a)).[26,56] The excess of oxygen plasma time in PEALD process also introduces the defect PL emissions related with zinc vacancies and other native defects.[25,39] These defects due to excess plasma time also produces broad emission band at around 600 nm.[38,52,53,57] Fig. 4(b) shows enhanced defect emissions in the PL spectrum with increasing oxygen plasma time (from 10 sec to 50 sec).

The sheet resistances of ZnO thin films grown on glass substrates with different plasma times were tested using standard four probe measurement. As oxygen plasma time was increase from 10 sec to 50 sec, sheet resistances of ZnO thin films were decreased from 10 MΩ/cm^2 (for 10 sec O_2 plasma) to 10 KΩ/cm^2 (for 50 sec O_2 plasma), nearly 3 order of magnitude (Fig. 4(c)). The mobility and carrier concentration of ZnO film were tested by standard hall bar configuration with DC bias. The estimated mobility and carrier concentration for the sample of 50 sec plasma time were 3.84 V · s/cm^2 and 2.5×10^{15} cm^{-3} (*p*-type), respectively. The resistances of other samples were too high to perform reliable Hall measurement. This reduction of sheet resistance of PEALD ZnO thin films may be attributed to two main reasons. One is growth of ZnO nanocrystal grain size. As O_2 plasma time is extended, ZnO crystal size also increases as can be seen in FE-SEM images (Fig. 1). This bigger crystal size allows longer carrier's mean free path within the ZnO film layer.[58,59] And the other may be attributed to the excess of oxygen, which basically leads to Zn vacancy and broken intrinsic stoichiometry of ZnO. Indeed, high quality and strictly stoichiometry ZnO film is highly insulating. Generally, the electrical properties of ZnO films are highly dependent on the impurities, such as hydrogen and hydroxyl, which can be induced in ALD process.[25–30,37,60,61] Both hydrogen and hydroxyl in ZnO behave as shallow donors and lead to higher carrier concentration.[20] Annealing ZnO film can effectively remove such impurities. We found that annealing of our PEALD ZnO thin films typically induced increase of sheet resistance by a factor of 10.

We employed PEALD ZnO thin films as the electron conductive layers in inverted polymer solar cells to study the effect structural evolution of ZnO thin films on the electronic device operations. Well known P3HT:PCBM bulk heterojunction film was used as an active layer of polymer solar cell. Fig. 5(a) and 5(b) display device structure for the fabricated inverted polymer solar cell structure and schematic for the photovoltaic process in our devices, respectively. Unlike conventional polymer solar cell, the generated electrons are collected in ITO cathode, whereas the generated holes are collected in top Au electrode in inverted polymer cell. ZnO thin film in this device configuration functions as an electron conducting layer (or hole blocking layer) by selective charge collection at the interface. Photovoltaic performance was measured under AM 1.5 illumination for a series of inverted polymer solar cells using ZnO films grown by different O_2 plasma times. The characteristic parameters of current-voltage curves for those solar cells are summarized in Table I. All values in Table II are averaged figures over 10 cell samples. The inverted polymer solar cells based on ZnO sol-gel films were also tested as a standard for comparison. According to surface images and XRD analyses, ZnO thin film evolved into more distinct hexagonal wurzite phase along (002) direction with increasing oxygen plasma time. But the enhanced overall structural order of ZnO thin film did not improve either open circuit voltage (V_{oc}) or short circuit current (I_{sc}) in current-voltage characteristic of inverted polymer cell as shown in Fig. 5 and Table II. Moreover, the Fill Factors (*FF*) were gradually reduced as the O_2 plasma time was increased from 20 sec to 50 sec. Especially

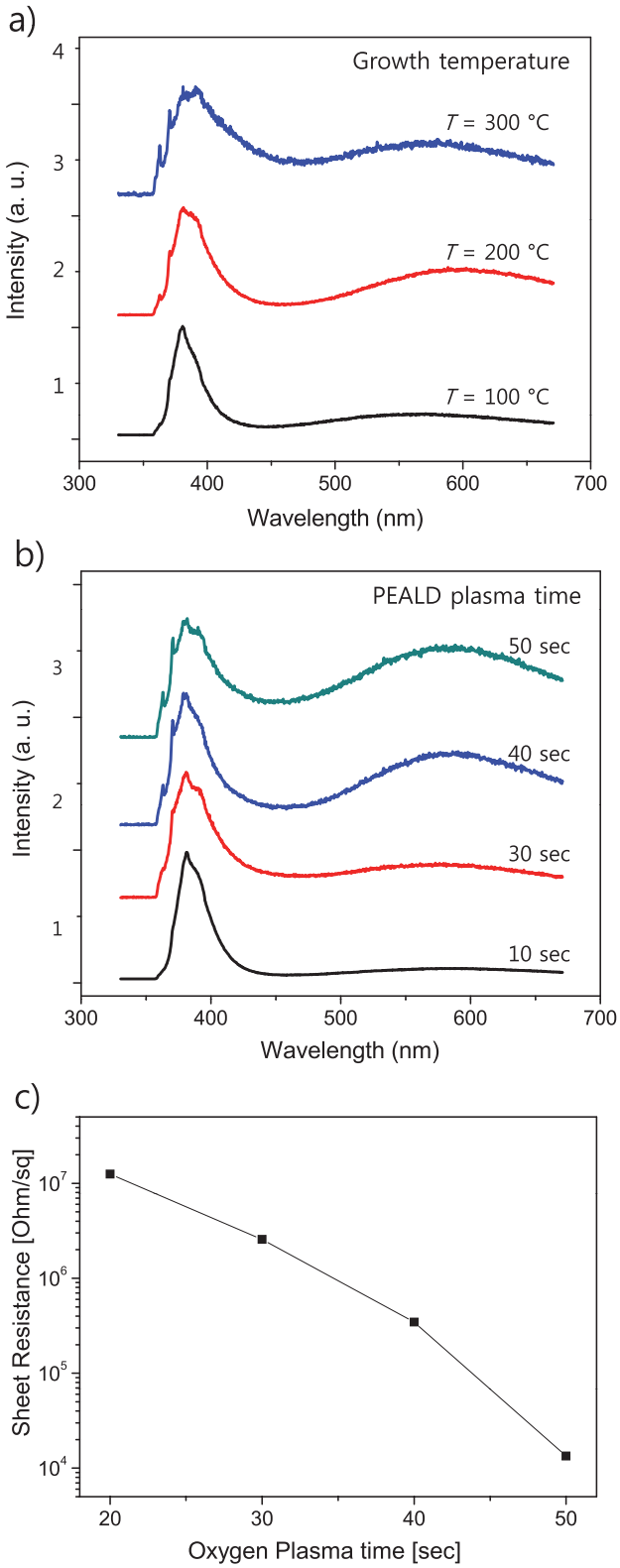

FIG. 4. (a) PL spectra of ZnO films depending on growth temperature from 100 to 300 °C with 100 °C interval. (b) PL spectra of ZnO films depending on O_2 plasma time from 10 sec to 50 sec with 10 sec interval. Both increasing growth temperature and plasma time enhance broad band emission around (500 nm – 700 nm). (c) Sheet resistance of ZnO films depending on O_2 plasma time. As the plasma time is increased, sheet resistance of sample was decreased by 3 orders of magnitude.

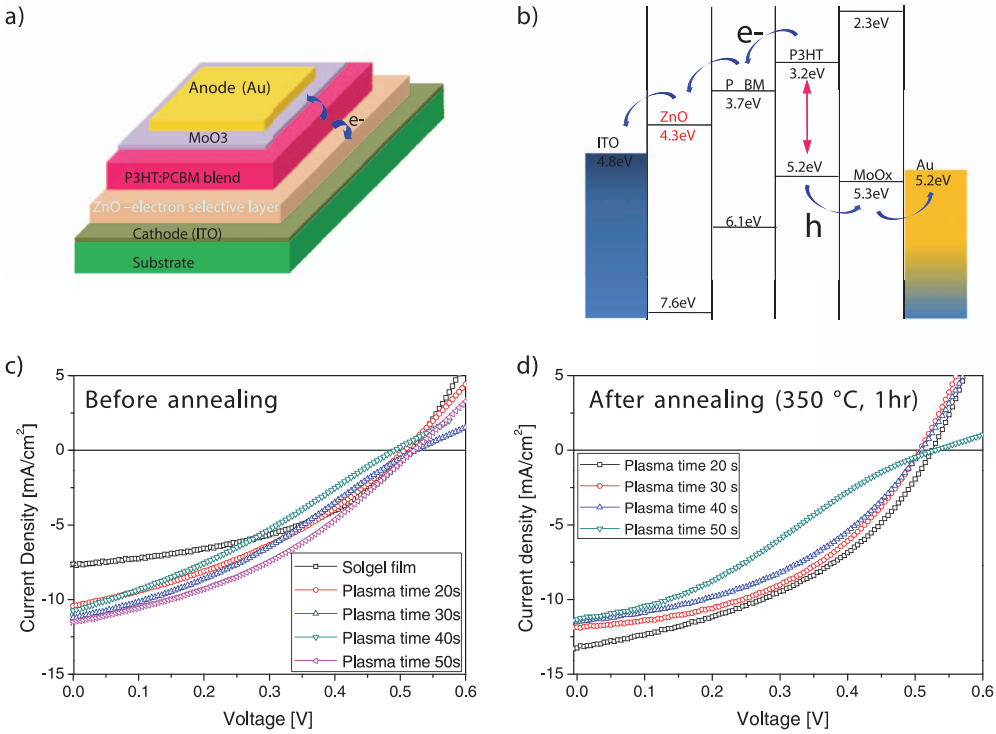

FIG. 5. (a) Device structure of our inverted polymer solar cell with ZnO film as an electron conductive layer. (b) Schematic for the current generation in our inverted polymer solar cell. The generated electrons are collected at ITO cathode through ZnO layer, whereas the generated holes are collected at Au anode thorough the MoO_x buffer layer. (c) The characteristic *I-V* curves for the cell devices fabricated with PEALD ZnO films grown by different O_2 plasma time (20 sec–50 sec) (b) The characteristic *I-V* curves for the cell devices fabricated after annealing of ZnO thin film at 350 °C for 1hr.

samples with 50 sec O_2 plasma time for ZnO growth exhibited significant fall down of *FF* as shown in Fig. 5 and Table II. It should be also emphasized that the sheet resistances of ZnO films significantly drop as the O_2 plasma time increased (Fig. 4(c)). The role of enhanced conductivity of ZnO thin film may be trivial in effective electron collection in inverted polymer solar cell. The substantial reduction of *FF* may be attributed to the Zn vacancies or other impurities (such as oxygen interstitials and space point defects) induced from excess plasma time. The pristine ZnO has direct band gap of 3.37 eV. But plasma induced Zn vacancies and other impurity defects can creates a number of deep levels, which could build an inter energy band. The formation of inter band in ZnO film can interrupt not only immediate exciton seperation but also selective charge collection at the interface.[52] Therefore, ZnO film which has those defects cannot work properly as an electron conductive buffer layer (or a hole barrier) in the inverted polymer solar cell. Fig. 5(c) and 5(d) display characteristic current-voltage curves for a series of cell devices with ZnO films grown by different plasma times. The variation of plasma time from 20 sec to 40 sec did not introduce substantial change in overall current-voltage curves. But samples of 50 sec plasma time clearly displayed significant drops in *FF* and cell efficiencies (distorted diode curve). A sudden decrease of photovoltaic current density (Fig. 5(c) and 5(d), 50 sec oxygen plasma sample) near the open circuit voltage (V_{oc}) may originate from electron-hole pair recombination. Ineffective charge collection at the interface as well as electron-hole separation could enhance recombination, especially at low potential gradiaent in the active layer. This is also consistence with the PL spectra in Fig. 4(a) and 4(b), which display enhanced deep level emission band in ZnO film with increasing O_2 plasma time in deposition process. The PEALD ZnO films may also contains other impurities, such as C, H from diethyl residue. Although such impurities can affect electrical properties of ZnO films, they also interrupt photovoltaic process by trapping free carriers. These impurities in PEALD ZnO films can be effectively removed by annealing samples over 300 °C. Fig. 5(d) displays current-voltage curves for a series of cell

TABLE II. Characteristic parameters of current-voltage curves in inverted polymer solar cell devices (All data are averaged values over 10 set of cell devices).

	V_{oc} [V]	I_{sc} [mA]	J_{sc} [mA/cm^2]	Fill Factor	Efficiency [%]
Solgel film	0.5183	0.8867	7.3889	0.4339	1.6606
ALD plasma 20s	0.5238	1.3275	11.0625	0.3600	2.0885
ALD plasma 30s	0.5017	1.2343	10.2861	0.3411	1.7630
ALD plasma 40s	0.5250	1.2580	10.4833	0.3234	1.7805
ALD plasma 50s	0.4863	1.1225	9.3542	0.2997	1.3699
ALD plasma 20s, 350 °C, 1hr annealed	0.4741	1.5128	12.6050	0.5096	3.6175
ALD plasma 30s, 350 °C, 1hr annealed	0.5493	1.3330	11.1050	0.5067	3.0868
ALD plasma 40s, 350 °C, 1hr annealed	0.5462	1.3170	10.9750	0.5101	3.0485
ALD plasma 50s, 350 °C, 1hr annealed	0.5313	1.3298	11.0813	0.3234	1.9011

devices fabricated after annealing ZnO thin film at 350 °C/1hr. Overall cell efficiencies and other characteristic parameters (I_{sc}, *FF*) were increased for a series of cell devices fabricated on annealed ZnO thin films. (see Fig. 5(c) and 5(d)). Even through annealing ZnO thin films can effectively remove residual impurities, Zn vacancies and other defects are likely still exist in the films. Therefore, annealing the samples of 50 sec plasma time do not improve *FF* and characteristic current-voltage curves as shown in Fig. 5(c) and 5(d).

In summary, ZnO thin films with controlled structural and electronic properties by PEALD process were incorporated into inverted polymer solar cell. In assessing photovoltaic performance of solar cell, V_{oc}, I_{sc}, and *FF* are generally considered as the most important factors. According to deposition conditions of ZnO films in PEALD process, there were huge differences in I_{sc} and *FF* of cell devices based on ZnO films even though their V_{oc} remained at almost same value of 0.5 V or less. Above all, sample's fill factors (*FF*) were significantly varied depending on oxygen plasma time (from 0.53 to 0.34) as shown in *I-V* curves (Fig. 5) and summarized data (Table II). Although annealing ZnO films induced significant increase of sheet resistances, it introduced substantial improvement on I_{sc} and *FF* for all series of devices. And the lowest *FF* (0.34) was obtained for the samples with ZnO films grown by 50 sec O_2 plasma time, which can be attributed to the significant modification of electronic configuration of ZnO film due to a large number of defects. Highest efficiency of $\eta = 4.08$ % with $Jsc = 13.28$ mA/cm^2, $V_{oc} = 0.49$ V, and $FF = 0.53$ was obtained for the annealed cell devices with ZnO film grown by 20 sec O_2 plasma time.

IV. CONCLUSION

Highly tunable structural and electronic properties of ZnO thin films were obtained using PEALD method. With relatively simple modification of deposition process, ZnO films display substantial evolution in the wide range of structural and physical properties, such as growth of nano crystal, surface roughness, photoluminescence, sheet resistance, etc. This readily tunable ability for the ZnO thin film growth is highly desirable since ZnO film has been under intense research for various device applications. We implemented these tunable ZnO films into inverted polymer solar cells and studied how the change in structural and optical properties of ZnO films affects on the photovoltaic device operations. Our results showed that structural and optical properties rather than electrical conductivities of ZnO thin film are more important factors for the optimal photovoltaic device operation.

ACKNOWLEDGMENT

This work was supported by a grant from (Future Challenge Project or Creativity and Innovation Project) funded by the UNIST (Ulsan National Institute of Science and Technology) and the year of 2011 research fund of the UNIST (Ulsan National Institute of Science and Technology). This research was also supported by Basic Science Research Program through the National

Research Foundation of Korea (NRF) funded by the Ministry of Education, Science and Technology (No. 2011-0014651)

[1] S.-M. Lukas and L. M-.D. Judith, "ZnO – nanostructures, defects, and devices," Materialstoday **5**, 40–48 (2007).
[2] A. B. Djurišić and Y. H. Leung, Small **2**, 944–961 (2006).
[3] Akhtar, M. R. Saeed, N. Saira, N. Rabia, and Shahzad, Adv. Sci. Lett. **19**, 834–838 (2013).
[4] A. K. K. Kyaw, X. W. Sun, C. Y. Jiang, G. Q. Lo, D. W. Zhao, and D. L. Kwong, Appl. Phys. Lett. **93**, 221107 (2008).
[5] Q. Zhang, C. S. Dandeneau, X. Zhou, and G. Cao, Adv. Mater. **21**, 1–22 (2009).
[6] J.-T. Jang, H. Ryu, and W.-J. Lee, Appl. Surf. Sci. **276**, 558–562 (2013).
[7] Z. L. Wang and J. Song, Science **312**, 242–246 (2006).
[8] Y. M. Niquet, Nano Letters **7**, 1105–1109 (2007).
[9] Y. Qin, X. Wang, and Z. L. Wang, Nature **451**, 809–813 (2008).
[10] M. Alexe, S. Senz, M. A. Schubert, D. Hesse, and U. Gosele, Adv. Mater. **20**, 4021–4026 (2008).
[11] M.-Y. Choi, D. Choi, M.-J. Jin, I. Kim, S.-H. Kim, J.-Y Choi, S. Y. Lee, J. M. Kim, and S.-W. Kim, Adv. Mater. **21**, 2185–2189 (2009).
[12] H. Sun, H. Tian, Y. Yang, D. Xie, Y.-C. Zhang, X. Liu, S. Ma, H.-M. Zhao, and T.-L. Ren, Nanoscale **5**, 6117 (2013).
[13] N. R. Aghamalyan, T. A. Aslanyan, E. S. Vardanyan, E. A. Kafadaryan, R. K. Hovsepyan, S. I. Petrosyan, and A. R. Poghosyan, J. Contemp. Phys. (American Academy of Sciences) **48**, 93–97 (2013).
[14] J. Erhart, Phys. Ics. Edu. **48**, (2013).
[15] C. S. Wei, Y. Y. Lin, Y. C. Hu, C. W. Wu, C. K. Shih, C. T. Huang, and S. H. Chang, Sens. Actuators. A **128**, 18–24 (2006).
[16] S. B. Lang, Phys. Today **58**(8), 31 (2005).
[17] C. Wang, X. Chu, and M. Wu, Sens. Actuators. B: Chem. **113**, 320–323 (2006).
[18] X. Jiaqiang, C. Yuping, C. Daoyong, and S. Jianian, Sens. Actuators. B **113**, 526–531 (2006).
[19] A. Tsukazaki, A. Ohtomo, T. Onuma, M. Ohtani, T. Makino, M. Sumiya, K. Ohtani, S. F. Chichibu, S. Fuke, Y. Segawa, H. Ohno, H. Koinuma, and M. Kawasaki, Nat. Mater. **4**, 42–46 (2005).
[20] L. Zhang, Y. Jiang, Y. Ding, M. Povey, and D. York, J. Nanopar. Res. **9**, 479–489 (2007).
[21] N. Padmavathy and R. Vijayaraghavan, Sci. Tech. Adv. Mater. **9**, 035004 (2008).
[22] C.-C. Huang, R. S. Aronstam, D.-R. Chen, and Y.-W. Huang, Toxicol. in Vitro **24**, 45–55 (2010).
[23] W. Lin, Y. Xu, C-.C. Huang, Y. Ma, K. B. Shannon, D.-R. Chen, and Y.-W. Huang, J. Nanopart. Res. **11**, 25–39 (2009).
[24] V. Miikkulainen, M. Leskelä, M. Ritala, and R. L. Puurunen, J. Appl. Sci. **113**, 021301 (2013).
[25] M. A. Thomas and J. B. Cui, ACS Appl. Mater. & Inter **4**, 3122–3128 (2012).
[26] B. P. Zhanga, K. Wakatsukia, N. T. Binha, N. Usamic, and Y. Segawaa, Thin Solid Films **449**, 12–19 (2004).
[27] H. Cheun, F.-H. Canek, Y. Zhou, W. J. Potscavage, S.-J. Kim, J. Shim, A. Dindar, and B. Kippelen, J. Phys. Chem. C **114**, 20713–20718 (2010).
[28] J.-C. Wang, W.-T. Weng, M.-Y. Tsai, M.-K. Lee, S.-F. Horng, T.-P. Perng, C.-C. Kei, C.-C. Yu, and H.-F. Meng, J. Mater. Chem. **20**, 862–866 (2010).
[29] C. Zhu, D. J. Smith, and R. J. Nemanich, J. Vac. Sci. Tech. B **30**, 051807 (2012).
[30] C. Marichy, M. Bechelany, and N. Pinna, Adv. Mater. **24**, 1017–1032 (2012).
[31] A. Savva and S. A. Choulis, Appl. Phys. Lett. **102**, 233301 (2013).
[32] A. Bikowski, T. Welzel, and K. Ellmer, Appl. Phys. Lett. **102**, 242106 (2013).
[33] T. Z. Oo, R. D. Chandra, N. Yantara, R. R. Prabhakar, L. H. Wong, N. Mathews, and S. G. Mhaisalkar, Org. Electron. **13**, 870 (2012).
[34] S. Ray, R. Das, and A. K. Barua, Sol. Ene rgy. Mater. Sol. Cells **74**, 387 (2002).
[35] M. J. Alam and D. C. Cameron, J. Vac. Sci. Tech. A **19**, 1642 (2001).
[36] A. Aprilia, P. Wulandari, V. Suendo, Herman, R. Hidayat, A. Fujii, and M. Ozaki, Sol. Energy Mater. Sol. Cells **111**, 181 (2013).
[37] Z. Zhou, K. Kato, T. Komaki, M. Yoshino, H. Yukawa, M. Morinaga, and K. Morita, J. Eur. Ceram. Soc. **24**, 139 (2004).
[38] L. E. Greene, M. Law, J. Goldberger, F. Kim, J. C. Johnson, Y. Zhang, R. J. Saykally, and P. Yang, Angew. Chem. Int. Edi. **42**, 3031 (2003).
[39] Ü. Özgür, Ya. I. Alivov, C. Liu, A. Teke, M. A. Reshchikov, S. Doğan, V. Avrutin, S.-J. Cho, and H. Morkoç, J. Appl. Phys. **98**, 041301 (2005).
[40] T. Krajewski, E. Guziewicz, M. Godlewski, L. Wachnicki, I. A. Kowalik, A. Wojcik-Glodowska, M. Lukasiewicz, K. Kopalko, V. Osinniy, and M. Guziewicz, Microelectron. J. **40**, 293 (2009).
[41] M. Godlewski, Microelectron. Eng. **85**, 2434 (2008).
[42] M. Godlewski, E. Guziewicz, G. Luka, T. Krajewski, M. Lukasiewicz, L. Wachnicki, A. Wachnicka, K. Kopalko, A. Sarem, and B. Dalati, Thin Solid Films **518**, 1145 (2009).
[43] M. S. White, D. C. Olson, S. E. Shaheen, N. Kopidakis, and D. S. Ginley, Appl. Phys. Lett. **89**, 143517 (2006).
[44] Y. Sahin, S. Alem, R. de Bettignies, and J. M. Nunzi, Thin Solid Films **476**, 340 (2005).
[45] M. Y. Song, K. J. Kim, and D. Y. Kim, Sol. Energy Mater. Sol. Cells **85**, 31 (2005).
[46] A. Watanabe and A. Kasuya, Thin Solid Films **483**, 358 (2005).
[47] C.-Y. Chang and F.-Y. Tsai, J. Mater. Chem. **21**, 5710–5715 (2011).
[48] C. Magne, T. Moehl, M. Urien, M. Gratzel, and T. Pauporté, J. Mater. Chem. A **1**, 2079–2088 (2013).
[49] A. K. K. Kyaw, D. H. Wang, D. Wynands, J. Zhang, T.-Q. Nguyen, G. C. Bazan, and A. J. Heeger, Nano Letters **13**, 3796–3801 (2013).
[50] O. Nilsen, O. B. Karlsen, A. Kjekshus, and H. Fjellvåg, Thin Solid Films **515**, 4550–4558 (2007).
[51] F. Tuomisto and K. Saarinen, Phys. Rev. B **72**, 085206 (2005).
[52] A. Janotti and C. G. Van de Walle, Phys. Rev. B **76**, 165202 (2007).

[53] S. W. Kim, Sz. Fujita, M. S. Yi, and D. H. Yoon, Appl. Phys. Lett. **88**, 253114 (2006).
[54] A. B. Djurisic and Y. H. Leung, Small **2**, 944 (2006).
[55] M.-J. Jin, S.-D. Lee, K.-S Shin, S.-W. Jeong, D. H. Yoon, D. Jeon, I.-H. Lee, D. K. Lee, and S.-W Kim, J. Nanosci. and Nanotech. **9**, 1–4 (2009).
[56] S. C. Lyu, Y. Zhang, H. Ruh, H.-J. Lee, H.-W. Shim, E.-K. Suh, and C. J. Lee, Chem. Phys. Lett. **363**, 134–138 (2002).
[57] S. W. Kim, M. Ueda, M. Funato, Sg. Fujita, and Sz. Fujita, J. Appl. Phys. **97**, 104316 (2005).
[58] M. P. Seah and W. A. Dench, Surf. Interface Anal. **1**, 1–10 (1979).
[59] W. Zhang, S. H. Brongersma, O. Richard, B. Brijs, R. Palmans, L. Froyen, and K. Maex, Microelectron. Eng. **76**, 146–152 (2004).
[60] C. G. Van de Walle, Phys. Rev. Lett. **85**, 1012–1015 (2000).
[61] Z. Zhou, K. Kato, T. Komaki, M. Yoshino, H. Yukawa, M. Morinaga, and K. Morita, J. Eur. Ceram. Soc. **24**, 139–146 (2004).